

DECLINING ROTATION CURVES AT $Z = 2$: A NATURAL PHENOMENON IN Λ CDM COSMOLOGY

ADELHEID F. TEKLU^{1,2}, RHEA-SILVIA REMUS^{1,3}, KLAUS DOLAG^{1,4}, ALEXANDER ARTH^{1,5},
ANDREAS BURKERT^{1,5}, AURA OBREJA¹, & FELIX SCHULZE^{1,5}

¹ Universitäts-Sternwarte München, Scheinerstraße 1, D-81679 München, Germany

² Excellence Cluster Universe, Boltzmannstraße 2, D-85748 Garching, Germany

³ Canadian Institute for Theoretical Astrophysics, 60 St. George Street, University of Toronto, Toronto ON M5S 3H8, Canada

⁴ Max-Planck Institute for Astrophysics, Karl-Schwarzschild-Str. 1, D-85741 Garching, Germany

⁵ Max-Planck Institute for Extraterrestrial Physics, Giessenbachstraße 1, D-85748 Garching, Germany
ateklu@usm.lmu.de

Draft version October 15, 2018

ABSTRACT

Selecting disk galaxies from the cosmological, hydrodynamical simulation *Magneticum Pathfinder* we show that almost half of our poster child disk galaxies at $z = 2$ show significantly declining rotation curves and low dark matter fractions, very similar to recently reported observations. These galaxies do not show any anomalous behavior, reside in standard dark matter halos and typically grow significantly in mass until $z = 0$, where they span all morphological classes, including disk galaxies matching present day rotation curves and observed dark matter fractions. Our findings demonstrate that declining rotation curves and low dark matter fractions in rotation dominated galaxies at $z = 2$ appear naturally within the Λ CDM paradigm and reflect the complex baryonic physics, which plays a role at the peak epoch of star-formation. In addition, we find that dispersion dominated galaxies at $z = 2$, which host a significant gas disk, exhibit similar shaped rotation curves as the disk galaxy population, rendering it difficult to differentiate between these two populations with currently available observation techniques.

Subject headings: dark matter – galaxies: evolution – galaxies: formation – galaxies: halos – hydrodynamics – methods: numerical

1. INTRODUCTION

Since the postulation of dark matter (DM) by Zwicky (1933), many observational studies analyzing rotation curves of galaxies (e.g. Rubin et al. 1978) have supported this picture: While rotational velocities (V^{rot}) deduced from the visible matter should decrease proportional to $r^{-1/2}$ in the outer parts of galaxies, they were found to remain flat. The awareness of this discrepancy in the mass content and thus the need for an explanation for this missing mass lead to the acceptance of dark matter as the dominant mass component of galaxies (see Naab & Ostriker (2017) for a detailed review).

Recently, Genzel et al. (2017) (see also Lang et al. 2017) presented measurements of rotation curves at redshift $z \approx 2$ that do not stay flat but decrease with increasing radius, opening a debate about the importance and even presence of DM in the outer disks and inner halos of these massive systems (and generally at higher redshift). In this letter we investigate whether the existence of decreasing rotation curves at high redshifts contradicts or actually is a natural outcome of the Λ CDM paradigm, using the state-of-the-art cosmological simulation *Magneticum Pathfinder*¹ (K. Dolag et al., in preparation).

2. THE SIMULATIONS

The *Magneticum Pathfinder* simulations are a set of state-of-the-art, cosmological, hydrodynamical simulations of different cosmological volumes with different resolutions. They follow a standard Λ CDM cosmology with parameters (h , Ω_M , Ω_Λ , Ω_b , σ_8) set to (0.704, 0.272,

0.728, 0.0451, 0.809), adopting a WMAP 7 cosmology (Komatsu et al. 2011).

These simulations follow a wide range of physical processes (see Hirschmann et al. 2014; Teklu et al. 2015, for details) which are important for studying the formation of active galactic nuclei (AGN), galaxies, and galaxy cluster. The simulation set covers a huge dynamical range with a detailed treatment of key physical processes that are known to control galaxy evolution, thereby allowing to reproduce the properties of the large-scale, intra-galactic, and intra-cluster medium (see e.g. Dolag et al. 2016; Gupta et al. 2017; Remus et al. 2017a) as well as the detailed properties of galaxies including morphological classifications and internal properties (see e.g. Teklu et al. 2015; Remus et al. 2017b; Teklu et al. 2017). This also includes the distribution of different chemical species within galaxies and galaxy clusters (Dolag et al. 2017), and the properties of the AGN population within the simulations (Hirschmann et al. 2014; Steinborn et al. 2016).

For this study we use the simulation *Box4/ubr*, which covers a volume of (68 Mpc)³, initially sampled with $2 \cdot 576^3$ particles (dark matter and gas), leading to a mass resolution of $m_{\text{gas}} = 7.3 \cdot 10^6 M_\odot$ for the gas and $m_{\text{stars}} = 1.8 \cdot 10^6 M_\odot$ for stellar particles, with a gravitational softening of $0.7 h^{-1} \text{kpc}$.

3. SAMPLE OF GALAXIES

To ensure proper resolution of the inner structure, we only select halos with virial masses above $5 \cdot 10^{11} M_\odot$ hosting galaxies with stellar masses above $5 \cdot 10^{10} M_\odot$ for this study. These mass ranges are consistent with

¹ www.magneticum.org

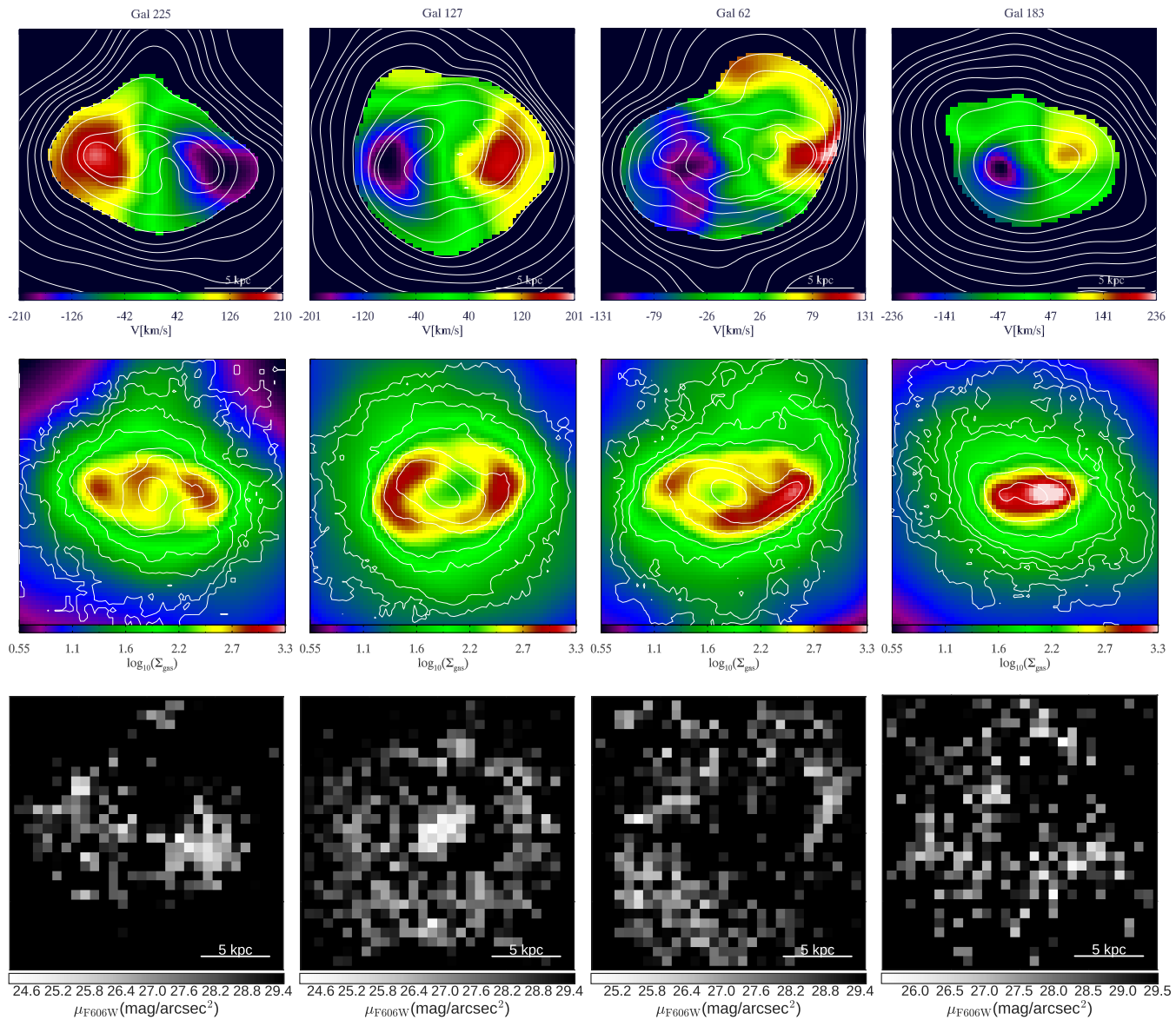


FIG. 1.— Example galaxies from the $z = 2$ sample with declining rotation curves (see Fig. 2), from left to right the three disk galaxies *gal 225*, *gal 127*, and *gal 62*, and the gas-rich spheroidal system *gal 183*, rotated to inclinations (e.g. $i = 60$, $i = 45$, $i = 25$ and $i = 75$, respectively) similar to those of the galaxies presented in Genzel et al. (2017). *Upper row:* Velocity maps of the cold gas component for each galaxy, with contours of the cold gas column density overlaid. *Middle row:* Cold gas column density maps with overlaid stellar column density contours. *Lower row:* Simulated HST broadband F606W images using *GRASIL-3D*.

the observed properties of the high- z galaxy sample of Genzel et al. (2017). This leads to a sample of 212 and 275 halos at $z = 2$ and $z = 0$, respectively. Furthermore, we classify the galaxies based on the distribution of the circularity parameter $\varepsilon = j_z/r\sqrt{GM(r)}/r$ of the stars within the galaxies, where j_z is the z -component of the stars' specific angular momentum (see also Abadi et al. 2003; Scannapieco et al. 2008). Thus, dispersion-dominated systems represent observed early-type galaxies and are characterized by a broad peak in the distribution at $\varepsilon \simeq 0$, while rotation-supported systems have properties that are characteristic of late-type galaxies and show a broad peak at $\varepsilon \simeq 1$. We define poster child disk galaxies as systems which, in addition to a characteristic peak at $\varepsilon \simeq 1$, have a significant cold gas fraction ($f_{\text{cold}} > 0.5$ at $z = 2$ and $f_{\text{cold}} > 0.2$ at $z = 0$) to distinguish them from transition type systems or on-

going merger events (for details see Teklu et al. 2015). For our simulations it has been shown that, following this classification scheme, galaxies of these two populations reproduce accordingly the observed stellar-mass-angular-momentum-relation (Teklu et al. 2015) and its evolution (Teklu et al. 2016), the mass-size relation and its evolution (Remus et al. 2017b), as well as the fundamental plane distributions (Remus & Dolag 2016).

We then rotate the galaxies such that the minor axis of the gas² is aligned with the z -axis, so that we can extract the rotation curve without any further modifications.

From the total of 212 (275) galaxies at $z = 2$ ($z = 0$) we classify 26 (15) as poster child disks, which we consider for further analysis. In addition, among our 27 poster

² Note that this is different from the computation for the classification, where the galaxies are rotated into the frame where the angular momentum vector of the stars is aligned with the z -axis.

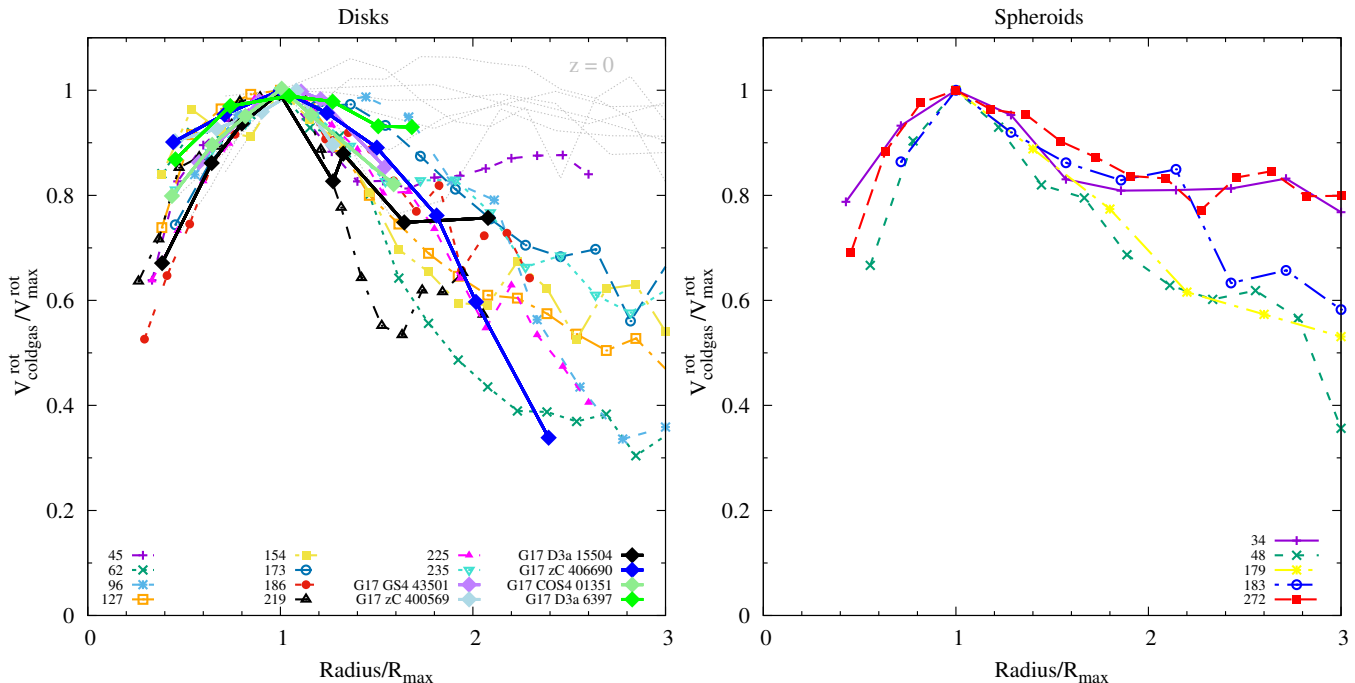


FIG. 2.— Rotation curves obtained from the cold gas for 10 out of the 26 poster child disk galaxies which show clearly declining rotation curves (left panel) and for the 5 gas-rich spheroidal galaxies (right panel) at $z = 2$, normalized by $V_{\text{coldgas}}^{\text{rot}}$ at the radius of maximum velocity R_{max} . The thick colored lines in the left panel show the 6 declining rotation curves presented in Genzel et al. (2017), while the gray lines show 7 poster child disk galaxies at $z = 0$, using $\approx 1.4 \cdot R_{1/2}$ as R_{max} .

child spheroidal galaxies at $z = 2$ we find 5 systems with a large cold gas fraction ($f_{\text{cold}} > 0.5$).

Fig. 1 shows a 20 kpc region for 4 gas-rich example galaxies at $z = 2$, where the upper row displays the line-of-sight velocity maps of the cold gas component, restricted to regions with $\Sigma_{\text{gas}} > 50 \frac{M_{\odot}}{\text{pc}^2}$, with overlaid cold gas column density contours. The gridded data was created using SPHMapper (Arth & Roettgers, in prep.). The middle row shows the cold gas column density maps with overlaid stellar surface density contours. Inclinations and colors were chosen according to the observations presented in Genzel et al. (2017). Each column represents one galaxy, where *gal 225*, *gal 127*, and *gal 62* (from left to right) resemble disk galaxies, while *gal 183* is a gas-rich spheroidal galaxy. Interestingly, all galaxies, even the spheroidal one, show a similar, regular rotation pattern for the cold gas component. This is due to the fact that the gas is in a flattened, centrifugally supported disk, while the stars form a spheroid.

The lower panels show mock images of the four galaxies in the HST broadband F606W (4750A-7000A), which corresponds to rest-frame mid-UV. The images have been generated with the radiative transfer code *GRASIL-3D* (Domínguez-Tenreiro et al. 2014). This wavelength range traces the regions of very recent star formation, and the spheroidal galaxy shows a very similar mock image as the disks, hiding the real stellar morphology.

4. ROTATION CURVES AT $Z = 2$

The rotation curves for our galaxy sample are directly obtained from the averaged tangential velocities (i.e. the circular velocities) of the individual cold gas particles. In order to ensure that only gas within the disk contributes to the rotation curve, only particles within the z -range of $\pm 3\text{kpc}$ are used. While the $z = 0$ disk galaxies show

normal rotation curves, 12 out of the 26 poster child disk galaxies at $z = 2$ show a significantly declining rotation profile for their gas disk. However, we further remove 2 of the 12 examples from our detailed analysis, as they show remnants of recent merger activity.

The left panel of Fig. 2 shows the rotation curves for these 10 poster child disk galaxies at $z = 2$, which exhibit a decline in the rotation curve similar to the observed high- z disk galaxies presented in Genzel et al. (2017) (thick solid lines). Following the observations, we scaled the individual rotation curves by R_{max} and $V_{\text{max}}^{\text{rot}}$, where R_{max} is the radius at which the rotational velocity ($V_{\text{coldgas}}^{\text{rot}}$) has its maximum. We only plot radii larger than the resolution limit of our simulation, i.e., two times the gravitational softening length of the gas, which corresponds to $\approx 1.33\text{kpc}$ at $z = 2$. As can clearly be seen, the simulated galaxies show the same behaviour as the observed ones, with some having an even steeper decline in the rotation curves as the observed galaxies. For comparison, the rotation curves of 7 disk galaxies at $z = 0$ are shown as gray lines. The difference in profile shapes between high- z and present-day galaxies is clearly visible.

Since at high redshift galaxies are in general more gas-rich, we also plot the same curves for the 5 gas-rich spheroidal galaxies from our $z = 2$ sample in the right panel of Fig. 2. As for the disks, the gas shows a clear rotational pattern (see also example in Fig. 1), and all of our gas-rich spheroidal galaxies show a declining rotation curve similar to the observed disk galaxies. The only difference here is that the gas disks in the spheroidals are much smaller than the stellar spheroidal bodies, while the sizes are similar in the disk galaxy cases (see Fig. 1).

The high redshift HST images mainly show young stars, which morphologically closely resemble the gas

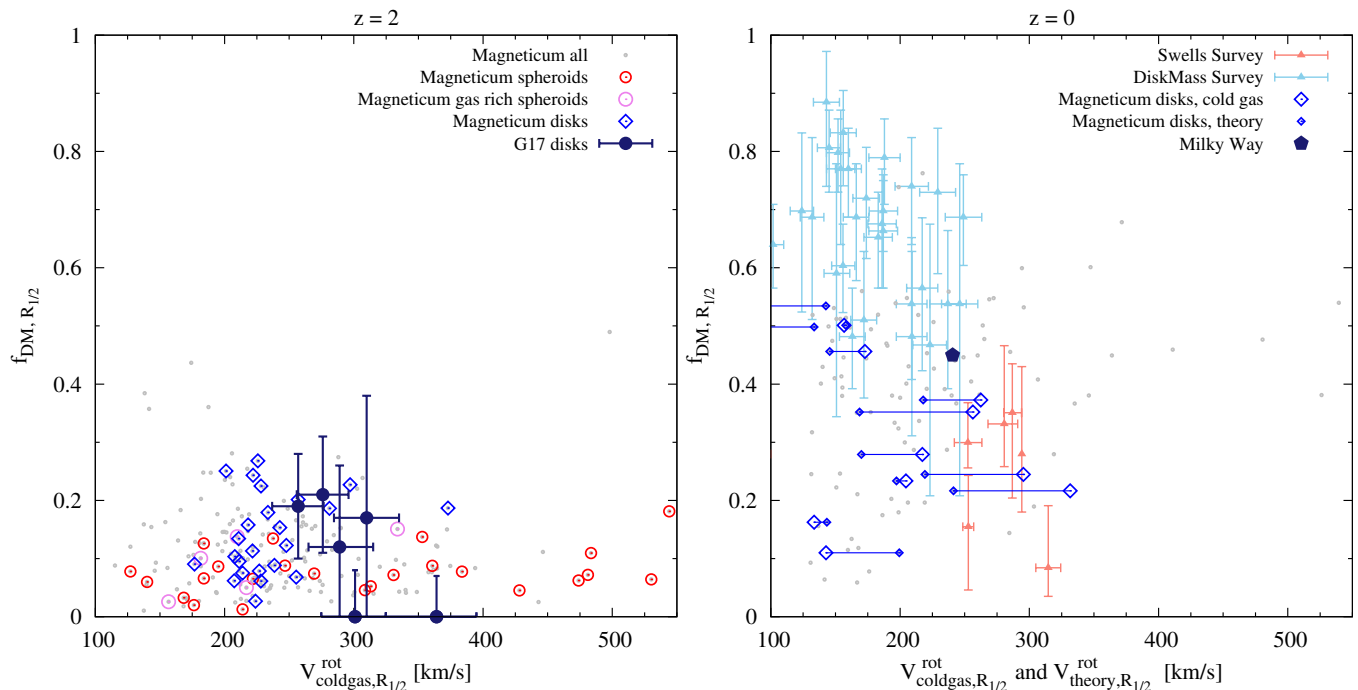


FIG. 3.— The DM fraction f_{DM} within the half-mass radius $R_{1/2}$ versus the rotational velocity $V_{\text{rot,coldgas},R_{1/2}}^{\text{rot}}$ at redshifts $z = 2$ (left) and $z = 0$ (right). At $z = 2$ (left panel), the simulated disks (blue diamonds) and gas-rich spheroidals (pink open circles) are shown together with the gas-poor spheroidals (red open circles). The observations from Genzel et al. (2017) are included as dark-blue points. At $z = 0$ (right panel), we only show the simulated disk galaxies, together with observations as presented in Courteau & Dutton (2015) from the Swells Survey (Barnabè et al. 2012; Dutton et al. 2013) and the DiskMass Survey (Martinsson et al. 2013). The dark-blue filled pentagon shows the Milky Way according to Bland-Hawthorn & Gerhard (2016). To indicate uncertainties involved in inferring $V_{\text{rot,coldgas},R_{1/2}}^{\text{rot}}$ we include for the simulated galaxies both the measured rotational gas velocity at $R_{1/2}$ as well as the theoretical value obtained from the total mass within $R_{1/2}$ and connect both points by blue lines.

disks even in the spheroidals (see lower panel of Fig. 1). This indicates a potential difficulty in distinguishing disk galaxies from gas-rich spheroidals at $z = 2$ observationally. However, this uncertainty should be resolved using the next generation of telescopes which will be able to probe the old stellar component in high redshift systems as well.

5. DM FRACTIONS

For spheroidal galaxies it is well known that the DM fraction within the half-mass radius is decreasing at higher redshift, which is commonly interpreted as indication for late growth by dry mergers of such systems. While this trend is qualitatively supported by cosmological simulations independent of the details in the implemented feedback models, the AGN feedback used in our simulation has been shown to produce DM fractions which quantitatively agree well with observations (see Remus et al. 2017b).

The left panel of Fig. 3 shows the DM fractions within the stellar half-mass radius $R_{1/2}$ for our full galaxy sample (gray dots) compared to observations at $z = 2$. Generally, our galaxies have a tendency for higher average DM fractions with decreasing $V_{\text{rot,coldgas}}^{\text{rot}}$, however, nearly all fractions are well below 30%. Our disk galaxies (blue diamonds) cover the same range of small DM fractions as the observations presented in Genzel et al. (2017) (dark-blue filled circles with error bars)³. Interestingly, the DM fractions of the disk systems are almost as small as

those of the spheroidal systems. Furthermore, the gas-rich spheroidals cover the same range in DM fractions as the observed and simulated disk galaxies, again highlighting the similarities between the gas-rich systems at $z = 2$ independent of their morphologies and demonstrating the difficulty in distinguishing pure rotation-dominated systems from dispersion-dominated systems which host a significant gas disk.

At $z = 0$ the disk galaxies in the simulations show much larger DM fractions which decrease with rotational velocity and agree well with the different measurements for disk galaxies (see right panel of Fig. 3). To indicate uncertainties involved in inferring $V_{\text{rot,coldgas},R_{1/2}}^{\text{rot}}$ we used both, the measured rotational gas velocity at $R_{1/2}$ as well as the theoretical values obtained by adopting centrifugal equilibrium and taking the total mass within $R_{1/2}$.

6. SURFACE DENSITY, DISPERSION AND THEORETICAL ROTATION CURVE

A detailed look at the four examples from Fig. 1 shows that the surface density profiles $\Sigma(r)$ of the cold gas disks in the three poster child disk galaxies and the gas-rich spheroidal galaxy follow the expected exponential decline, as shown in the upper panel of Fig. 4. While the theoretical rotation curves as obtained by the total matter distribution within these halos are flat, as expected, the real measured rotation of the cold gas disk shows a significant decline, as can be seen in the middle panel of

³ Note that especially at $z = 2$ the unavoidable differences when inferring the half-mass radius in simulations and observations could lead to noticeable differences.

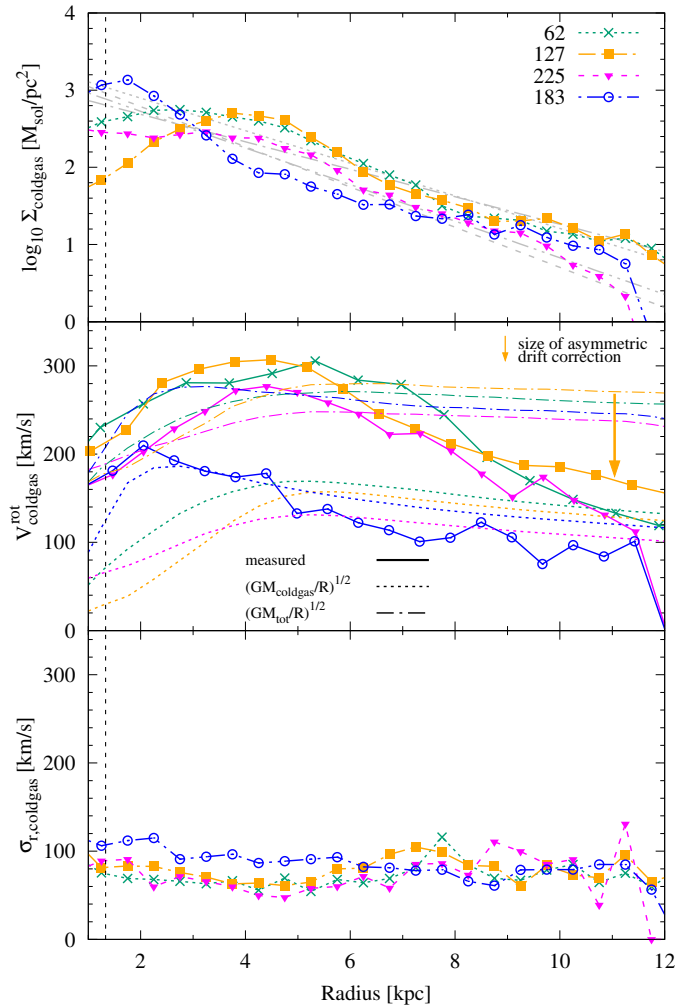


FIG. 4.— For the three poster child disks (*gal 62*, *gal 127*, and *gal 225*), and the gas-rich spheroidal galaxy (*gal 183*): *Upper panel*: Surface density Σ of the cold gas. The vertical dashed line indicates the resolution limit. The gray lines are fits for an exponential surface density profile for $\Sigma(x) = a \cdot \exp(-x/b)$ with $b \approx 2$ kpc. *Middle panel*: Rotation curves of the cold gas (solid lines) compared to the rotation curves expected from the spherically averaged total mass distribution (dash-dotted lines). Dotted lines show the corresponding cold gas contribution. The yellow arrow indicates exemplarily the size of the expected correction due to the asymmetric drift at large radii for galaxy *gal 62*. *Bottom panel*: Radial velocity dispersion σ_r of the cold gas.

Fig. 4. This decline is a result of the kinetic pressure effect which partly compensates the gravitational force as proposed by Burkert et al. (2010). As expected for a self-gravitating, exponential disk the maximum of the real rotation curve for the three disk galaxies is slightly ($\approx 10\%$) above the maximum value for a spherically averaged mass distribution. Furthermore, at large distances the real rotational velocity is conspiratorially close to the expected rotational velocity if considering only the cold gas mass. For the gas-rich spheroidal galaxy the latter holds even across almost all radii, due to its even lower DM fraction and the small size of the disk compared to the stellar body of the galaxy. As a result, the gaseous disk is strongly self-gravitating and more compact. None of our systems with a falling rotation curve shows any significant feature or change in the radial component of the velocity dispersion measured for the cold gas disk which

is related to the position at which the rotation curve declines, as shown in the σ_r profiles in the lower panel of Fig. 4.

7. DISCUSSION AND CONCLUSIONS

Selecting disk galaxies with M_{vir} above $5 \cdot 10^{11} M_{\odot}$ and M_{\star} above $5 \cdot 10^{10} M_{\odot}$ from the cosmological, hydrodynamical simulation *Magneticum Pathfinder* we investigated the rotation curves of disk galaxies at $z = 2$. We find that almost half of our poster child disk galaxies (10 out of 26) show significantly declining rotation curves, very similar to the observations reported in Genzel et al. (2017). Interestingly, the peak of the rotation curve is a fairly good approximation ($\approx 10\%$ larger) of the theoretical value, based on the total mass of the galaxies.

These disk galaxies do not show any significant dynamical features except that the radial dispersion has generally larger values compared to $z = 0$ disks. Applying a simple correction for the asymmetric drift (Burkert et al. 2010) based on our measured dispersion profiles onto the theoretical rotation curve results in reduced rotation curves, which qualitatively agree well with our measured ones. Therefore, we conclude that the declining rotation curves of the high redshift galaxies are caused by a relatively thick, turbulent disk, as already discussed in Genzel et al. (2017). We also find that these galaxies show similarly low DM fractions as reported for the observations. The DM halos of these disk galaxies have a mean concentration parameter $c_{\text{vir}} \approx 8$ (as expected for these halo masses at $z = 2$) and therefore we can exclude that the low dark matter fractions are caused by especially low concentrations of the underlying halos.

Tracing these galaxies in the simulations until $z = 0$ allows us to infer the present-day appearances of these galaxies. We find that, on average, these galaxies still grow by a factor of ≈ 3.5 both in virial as well as in stellar mass. Two of them resemble present-day disk galaxies with small remaining gas disks, and one ends as a central galaxy of a small group. Three of them become satellite galaxies of small groups, while the rest is mostly classified as transition types. Therefore, we can exclude that the low DM fractions at $z = 2$ imply that these systems have to be the progenitors of today's elliptical galaxies with similar stellar mass and low dark matter fractions.

Interestingly, in our simulations we also find several spheroidal galaxies at $z = 2$ which host a massive cold gas disk with similarly declining rotation curves as the disk galaxies. These gas disks are typically more compact, but as star formation is dominated by the gas disks, these spheroidals appear indistinguishable from the disk galaxies in our mock HST images, highlighting the need for observational instruments that detect the old stellar component even at high redshifts.

In general, we conclude that high-redshift disk galaxies with declining rotation curves and low DM fractions appear naturally within the Λ CDM paradigm, reflecting the complex baryonic physics which plays a role at $z = 2$ and can be found commonly in state-of-the-art, Λ CDM cosmological hydrodynamical simulations.

We thank Tadzju Hoffmann for useful discussions. AFT and KD are supported by the DFG Transregio TR33, AB is supported by the DFG Priority Programme

1573. AO has been funded by the Deutsche Forschungsgemeinschaft (DFG, German Research Foundation) – MO 2979/1-1. This research is supported by the DFG Cluster of Excellence “Origin and Structure of the Uni-

verse.” We are especially grateful for the support by M. Petkova through the Computational Center for Particle and Astrophysics (C2PAP). Computations have been performed at the ‘Leibniz-Rechenzentrum’ with CPU time assigned to the Project “pr86re.”

REFERENCES

- Abadi, M. G., Navarro, J. F., Steinmetz, M., & Eke, V. R. 2003, *ApJ*, 597, 21
- Barnabè, M., Dutton, A. A., Marshall, P. J., Auger, M. W., Brewer, B. J., Treu, T., Bolton, A. S., Koo, D. C., & Koopmans, L. V. E. 2012, *MNRAS*, 423, 1073
- Bland-Hawthorn, J. & Gerhard, O. 2016, *ARA&A*, 54, 529
- Burkert, A., Genzel, R., Bouché, N., Cresci, G., Khochfar, S., Sommer-Larsen, J., Sternberg, A., Naab, T., Förster Schreiber, N., Tacconi, L., Shapiro, K., Hicks, E., Lutz, D., Davies, R., Buschkamp, P., & Genel, S. 2010, *ApJ*, 725, 2324
- Courteau, S. & Dutton, A. A. 2015, *ApJ*, 801, L20
- Dolag, K., Komatsu, E., & Sunyaev, R. 2016, *MNRAS*, 463, 1797
- Dolag, K., Mevius, E., & Remus, R.-S. 2017, *Galaxies*, 5, 35
- Domínguez-Tenreiro, R., Obreja, A., Granato, G. L., Schurer, A., Alpresa, P., Silva, L., Brook, C. B., & Serna, A. 2014, *MNRAS*, 439, 3868
- Dutton, A. A., Treu, T., Brewer, B. J., Marshall, P. J., Auger, M. W., Barnabè, M., Koo, D. C., Bolton, A. S., & Koopmans, L. V. E. 2013, *MNRAS*, 428, 3183
- Genzel, R., Schreiber, N. M. F., Übler, H., Lang, P., Naab, T., Bender, R., Tacconi, L. J., Wisnioski, E., Wuyts, S., Alexander, T., Beifiori, A., Belli, S., Brammer, G., Burkert, A., Carollo, C. M., Chan, J., Davies, R., Fossati, M., Galametz, A., Genel, S., Gerhard, O., Lutz, D., Mendel, J. T., Momcheva, I., Nelson, E. J., Renzini, A., Saglia, R., Sternberg, A., Tacchella, S., Tadaki, K., & Wilman, D. 2017, *Nature*, 543, 397
- Gupta, N., Saro, A., Mohr, J. J., Dolag, K., & Liu, J. 2017, *MNRAS*, 469, 3069
- Hirschmann, M., Dolag, K., Saro, A., Bachmann, L., Borgani, S., & Burkert, A. 2014, *MNRAS*, 442, 2304
- Komatsu, E., Smith, K. M., Dunkley, J., Bennett, C. L., Gold, B., Hinshaw, G., Jarosik, N., Larson, D., Nolta, M. R., Page, L., Spergel, D. N., Halpern, M., Hill, R. S., Kogut, A., Limon, M., Meyer, S. S., Odegard, N., Tucker, G. S., Weiland, J. L., Wollack, E., & Wright, E. L. 2011, *ApJS*, 192, 18
- Lang, P., Förster Schreiber, N. M., Genzel, R., Wuyts, S., Wisnioski, E., Beifiori, A., Belli, S., Bender, R., Brammer, G., Burkert, A., Chan, J., Davies, R., Fossati, M., Galametz, A., Kulkarni, S. K., Lutz, D., Mendel, J. T., Momcheva, I. G., Naab, T., Nelson, E. J., Saglia, R. P., Seitz, S., Tacchella, S., Tacconi, L. J., Tadaki, K.-i., Übler, H., van Dokkum, P. G., & Wilman, D. J. 2017, *ApJ*, 840, 92
- Martinsson, T. P. K., Verheijen, M. A. W., Westfall, K. B., Bershady, M. A., Andersen, D. R., & Swaters, R. A. 2013, *A&A*, 557, A131
- Naab, T. & Ostriker, J. P. 2017, *ARA&A*, 55, 59
- Remus, R.-S. & Dolag, K. 2016, in *The Interplay between Local and Global Processes in Galaxies*,
- Remus, R.-S., Dolag, K., & Hoffmann, T. 2017a, *Galaxies*, 5, 49
- Remus, R.-S., Dolag, K., Naab, T., Burkert, A., Hirschmann, M., Hoffmann, T. L., & Johansson, P. H. 2017b, *MNRAS*, 464, 3742
- Rubin, V. C., Thonnard, N., & Ford, Jr., W. K. 1978, *ApJ*, 225, L107
- Scannapieco, C., Tissera, P. B., White, S. D. M., & Springel, V. 2008, *MNRAS*, 389, 1137
- Steinborn, L. K., Dolag, K., Comerford, J. M., Hirschmann, M., Remus, R.-S., & Teklu, A. F. 2016, *MNRAS*, 458, 1013
- Teklu, A. F., Remus, R.-S., & Dolag, K. 2016, in *The Interplay between Local and Global Processes in Galaxies*,
- Teklu, A. F., Remus, R.-S., Dolag, K., Beck, A. M., Burkert, A., Schmidt, A. S., Schulze, F., & Steinborn, L. K. 2015, *ApJ*, 812, 29
- Teklu, A. F., Remus, R.-S., Dolag, K., & Burkert, A. 2017, *MNRAS*, 472, 4769
- Zwicky, F. 1933, *Helvetica Physica Acta*, 6, 110